Acta Cryst. (1996). B52, 932–938

Synthesis and Structure Refinement of a New Type of Layered Intergrowth Phase: $Sb_{3+x}Nb_{3-x}TiO_{14}$ and $Sb_{3+x}Ta_{3-x}TiO_{14}$

CHRISTOPHER D. LING,[a]* SIEGBERT SCHMID,[a] JOHN G. THOMPSON,[a] RAY L. WITHERS[a] AND META STERNS[b]

[a]*Research School of Chemistry and* [b]*Department of Chemistry, Australian National University, Canberra, ACT 0200, Australia. E-mail: ling@rsc.anu.edu.au*

(*Received 20 December 1995; accepted 18 June 1996*)

Abstract

Attempts to synthesize Sb-based analogues of the known Bi-based Aurivillius phase, Bi_3TiNbO_9, have led to the discovery of an isomorphous pair of a new type of layered intergrowth phase of general stoichiometry $Sb_{3+x}Nb_{3-x}TiO_{14}$ and $Sb_{3+x}Ta_{3-x}TiO_{14}$. Electron diffraction proved essential for the initial recognition and structural characterization of these phases. The structures of $Sb_{3+x}Nb_{3-x}TiO_{14}$, $x = 0.89$, and $Sb_{3+x}Ta_{3-x}TiO_{14}$, $x = 1.26$, are reported. The structures are described as ordered intergrowths of β-Sb_2O_4-type and Sb_2O_5-type structures, with Nb^V/Ta^V substituting for Sb^V in the former and $Nb^V/Ta^V/Ti^{IV}$ substituting for Sb^V in the latter.

1. Introduction

Many complex layered phases, consisting of ordered intergrowths of slabs of simpler structure types, are known. The archetypal example is the bismuth oxide-based Aurivillius family of phases (Aurivillius, 1949). Within this family of phases, there exists a large number of displacive ferroelectrics (Subbarao, 1973; Singh, Bopardikare & Atkare, 1988) with room-temperature structures, which can be described in terms of relatively small amplitude, displacive modulations away from a high symmetry, prototype and parent structure (Rae, Thompson & Withers, 1991, 1992; Thompson, Rae, Withers & Craig, 1991). This $I4/mmm$, $a_p = b_p \simeq 3.85$ Å, c-prototype parent structure consists of perovskite-like $A_{n-1}B_nO_{3n+1}$ slabs regularly interleaved with α-PbO-type $Bi_2O_2^{2+}$ layers. The crystal chemistry underlying strong ferroelectricity in two of these Aurivillius phases ($Bi_4Ti_3O_{12}$ and Bi_3TiNbO_9) has been attributed to gross underbonding of the Bi^{3+} ions occupying the perovskite A site in the parent structure (Withers, Thompson & Rae, 1991).

While much work has been, and still is being, carried out on bismuth oxide-based phases other than Aurivillius phases, *e.g.* the so-called BIMEVOX and BICUVOX phases (Lee, Lim & West, 1994), relatively little work has been carried out on layered phases based on antimony oxides. Given that Sb is directly above Bi in the periodic table as well as having a stable 3+ valence state, it seems possible that direct antimony-based analogues to Aurivillius phases might exist. Recent attempts to completely substitute antimony for bismuth in several known Aurivillius phases (Castro, Millán & Martinez-Lope, 1993*a*,*b*; Castro, Millán, Enjalbert, Snoeck & Galy, 1994) were unsuccessful, with the exception of Sb_2WO_6 (Castro *et al.*, 1994; Ling, Withers, Rae, Schmid & Thompson, 1996) and Sb_2MoO_6 (Ling *et al.*, 1996).

While attempting to grow antimony-based analogues to the Aurivillius phase Bi_3TiNbO_9, a complex reaction product was obtained. Investigation *via* electron diffraction revealed the presence of an $A12/a1$, $a = 5.5$, $b = 4.8$, $c = 40$ Å phase. The stoichiometry was identified by energy-dispersive X-ray analysis (EDAX), in both a transmission electron microscope (TEM; Philips EM430) and a scanning electron microscope (SEM; JEOL 6400) as a solid-solution phase of general stoichiometry $Sb_{3+x}Nb_{3-x}TiO_{14}$, $0.6 \le x \le 1.3$. Subsequently, it proved possible to grow the tantalum-containing analogue with general stoichiometry $Sb_{3+x}Ta_{3-x}TiO_{14}$, $0.7 \le x \le 1.8$. Charge balance requires the presence of mixed-valence antimony; the general formulae may be written $Sb_3^{III}Sb_x^V(Nb,Ta)_{3-x}TiO_{14}$. While we have identified a composition range x for each solid solution based on EDAX analyses within the various specimens, the full extent of the solid solution has yet to be determined.

2. Experimental

Crystals of $Sb_{3+x}Nb_{3-x}TiO_{14}$ were grown by solid-state reaction of a mixture of Sb_2O_3 (Aldrich 99.99%), Nb_2O_5 (Koch-Lite 99.9%) and TiO_2 (Halewood 99.998%), heated with the mole ratio 4:2:1, in a sealed platinum tube, to 1423 K for 15 h then cooled to 1123 K over 15 h. Small, transparent, yellow plate-like crystals were formed on the surface of the specimen. Crystals of $Sb_{3+x}Ta_{3-x}TiO_{14}$ were grown in the same fashion (Aldrich 99.99% Ta_2O_5).

The crystal of $Sb_{3+x}Nb_{3-x}TiO_{14}$ chosen for X-ray data collection was selected using a transmission optical microscope with crossed polarizers and was free of any apparent microdomains. Given the almost endemic nature of twinning in the Aurivillius phases, it seemed

prudent to avoid similar problems here if possible. The cut crystal was a plate with the thin dimension corresponding to the crystallographic c^* axis. The absorption correction, $\mu(\text{Mo } K\alpha) = 12.63\ \text{mm}^{-1}$, used distances to the seven faces from an internal origin of (111) 0.106, $(0\bar{1}\bar{1})$ 0.120, (001) 0.009, $(00\bar{1})$ 0.009, $(\bar{1}1\bar{3})$ 0.108, $(1\bar{1}3)$ 0.114 and $(\bar{1}0\bar{2})$ 0.125 mm. The numerical correction used a $14 \times 14 \times 14$ grid. Data correlation using equivalent reflections was used to optimize the thin dimension.

The crystal of $Sb_{3+x}Ta_{3-x}TiO_{14}$ chosen for X-ray data collection was similarly selected and was also ostensibly free of microdomains. The cut crystal was a plate with the thin dimension corresponding to the crystallographic c^* axis. The absorption correction, $\mu(\text{Mo } K\alpha) = 30.94\ \text{mm}^{-1}$, used distances to the seven faces from an internal origin of $(\bar{1}12)$ 0.0208, $(\bar{2}\bar{1}3)$ 0.0144, $(1\bar{1}\bar{2})$ 0.0144, (001) 0.0030, $(00\bar{1})$ 0.0030, $(\bar{1}\bar{2}1)$ 0.0166 and $(22\bar{3})$ 0.0201 mm. The numerical correction used a $14 \times 14 \times 14$ grid.

In collecting both data sets, slight streaking of reflections was observed in ω-scan mode, suggesting that β varied across the crystals. This was attributed to variation of x, *i.e.* compositional variation within single crystals as observed by EDAX. Nonetheless, sufficiently good refinements were obtained with both data sets to suggest that this was a benign source of error and that the results were accurate averages for each crystal.

3. Results

3.1. *Electron diffraction*

Single crystal grains of $Sb_{3+x}Nb_{3-x}TiO_{14}$ and $Sb_{3+x}Ta_{3-x}TiO_{14}$ were studied by electron diffraction using Jeol 100CX and Philips EM430 TEMs. A monoclinic unit cell was identified; $a \simeq 5.5$, $b \simeq 4.8$, $c \simeq 40$ Å, $\beta \simeq 91°$. Given this long c axis and the low symmetry, it is not surprising that it was at first impossible to determine the unit cell or space-group symmetry from XRD. Microdiffraction patterns (DP's) taken down the (*a*) [100], (*b*) [010] and (*c*) [001] zone axes of $Sb_{3+x}Nb_{3-x}TiO_{14}$ are shown in Fig. 1. Note the absences hkl, $k+l$ = odd and $h0l$, h, l = odd; these extinction conditions are compatible with space-group symmetries $A1a1$ and $A12/a1$. DP's for $Sb_{3+x}Ta_{3-x}TiO_{14}$ were found to be entirely analogous. The standard monoclinic setting would require a and c to be switched; the non-standard setting used here was retained in accordance with the convention of labelling the stacking axis of layered structures c (the vertical axis of the solved structure in Fig. 2).

Although a c axis of approximately 40 Å is superficially consistent with an $n = 4$ Aurivillius phase (Subbanna, Ganapathi, Rao & Jefferson, 1986), such an interpretation is inconsistent with the pattern of reflection intensities seen in the [100] and [010] DP's; every seventh reflection along c^* (*i.e.* the allowed reflections $0,0,14n$, where n is an integer) is much stronger than the others. The pattern is shown more clearly in a systematic row DP (Fig. 1*d*), where multiple-diffraction routes through reciprocal lattice planes are not possible. This suggests a strongly scattering structural repeat along **z** of $c/14 \simeq 2.87$ Å, corresponding to the average metal-atom spacing in a layered structure. This average metal-atom spacing is inconsistent with an $n = 4$ Aurivillius phase.

3.2. *Structure solution and refinement of* $Sb_{3+x}Nb_{3-x}TiO_{14}$

Intensities for equivalent reflections were merged under $1m1$ and 121. Anomalous-dispersion corrected intensities merged to $R_1 = \Sigma|I_j - I|/\Sigma I_j = 0.028$ in both cases. As this indicated no advantage in using the non-centrosymmetric space group, the refinement was carried out in $A12/a1$.

A starting model for Sb-atom positions in the structure of $Sb_{3+x}Nb_{3-x}TiO14$ was obtained by direct methods. The remaining metal, and subsequently O, atoms were located *via* difference-Fourier synthesis. Potential mixed-atom sites were identified by calculating atomic valences [AV's (Brese & O'Keeffe, 1991)] for all possible occupancies of each metal-atom site (see Table 6). It was immediately apparent that the Sb1 and Sb2 sites could only be occupied by Sb^{3+} and that the additional antimony on the other metal-atom sites required by stoichiometry had to be in the 5+ valence state. Populations were refined by constraining thermal parameters of metal atoms on each site to be equal and sites to be fully occupied. Where refinement minimized the population of a metal, it was removed. The titanium population was constrained to 50% on the only site it was found to occupy, in accordance with overall charge balance requirements. The refined structure contained two mixed sites; $Sb^{V}_{0.36}Nb_{0.14}Ti_{0.5}$ and $Sb^{V}_{0.08}Nb_{0.92}$, giving an overall value for the solid solution coefficient x of 0.89 (within the range of EDAX observations).

Details of the diffraction experiment are given in Table 1. Final refined values for the fractional coordinates and mean-square atomic displacements $U_{eq} = (1/3)\Sigma_i\Sigma_j U_{ij} a_i^* a_j^* \mathbf{a}_i.\mathbf{a}_j$ of $Sb_{3+x}Nb_{3-x}TiO_{14}$ are given in Table 2, bond lengths in Table 3 and anisotropic atomic displacement parameters in Table 8.*

3.3. *Structure refinement of* $Sb_{3+x}Ta_{3-x}TiO_{14}$

The structure of $Sb_{3+x}Ta_{3-x}TiO_{14}$ was refined using the refined structure of $Sb_{3+x}Nb_{3-x}TiO_{14}$ as a starting model. AV's for potential occupants of all metal-atom sites are given in Table 7, demonstrating the same pattern of occupancies as for $Sb_{3+x}Nb_{3-x}TiO_{14}$ (see Table 6). Details of the diffraction experiment are given in Table

* A list of structure factors has been deposited with the IUCr (Reference: BR0050). Copies may be obtained through The Managing Editor, International Union of Crystallography, 5 Abbey Square, Chester CH1 2HU, England.

1. Mixed-atom site populations refined to similar values as for $Sb_{3+x}Nb_{3-x}TiO_{14}$,$Sb^{V}_{0.04}Ta_{0.46}Ti_{0.5}$ and $Sb^{V}_{0.59}Ta_{0.41}$, *i.e.* $x = 1.26$ (within the range of EDAX observations). Final refined values for the fractional coordinates and U_{eq} values of $Sb_{3+x}Ta_{3-x}TiO_{14}$ are given in Table 4, bond lengths in Table 5 and atomic displacement parameters in Table 9. Anisotropic atomic displacement parameters for O atoms did not refine reasonably, therefore, anisotropic parameters are reported for metal atoms only.

4. Discussion

Fig. 2 shows [100] and [010] zone-axis projections of the structure of $Sb_{3+x}Nb_{3-x}TiO_{14}$, plotted by the program *CrystalMaker* (Palmer, 1994). The coordinates of $Sb_{3+x}Ta_{3-x}TiO_{14}$ show it to be isostructural. From these projections, it is obvious that these are layered phases. There are in fact 14 discrete layers of metal atoms, approximately evenly spaced over the 40 Å *c* axis in accordance with the above electron diffraction evidence. The nature and arrangement of the intergrown slabs, however, are quite different to those found in the Aurivillius family of phases. Successive octahedral layers in the Sb^{V}(Nb,Ta)Ti, O4, O4, Sb^{V}(Nb,Ta)Ti, O7, O2 region of the structure, for example, have the edge-shared rutile configuration rather than the corner-shared perovskite configuration. A possible explanation for this may be the large (*ca* 25°) octahedral rotations

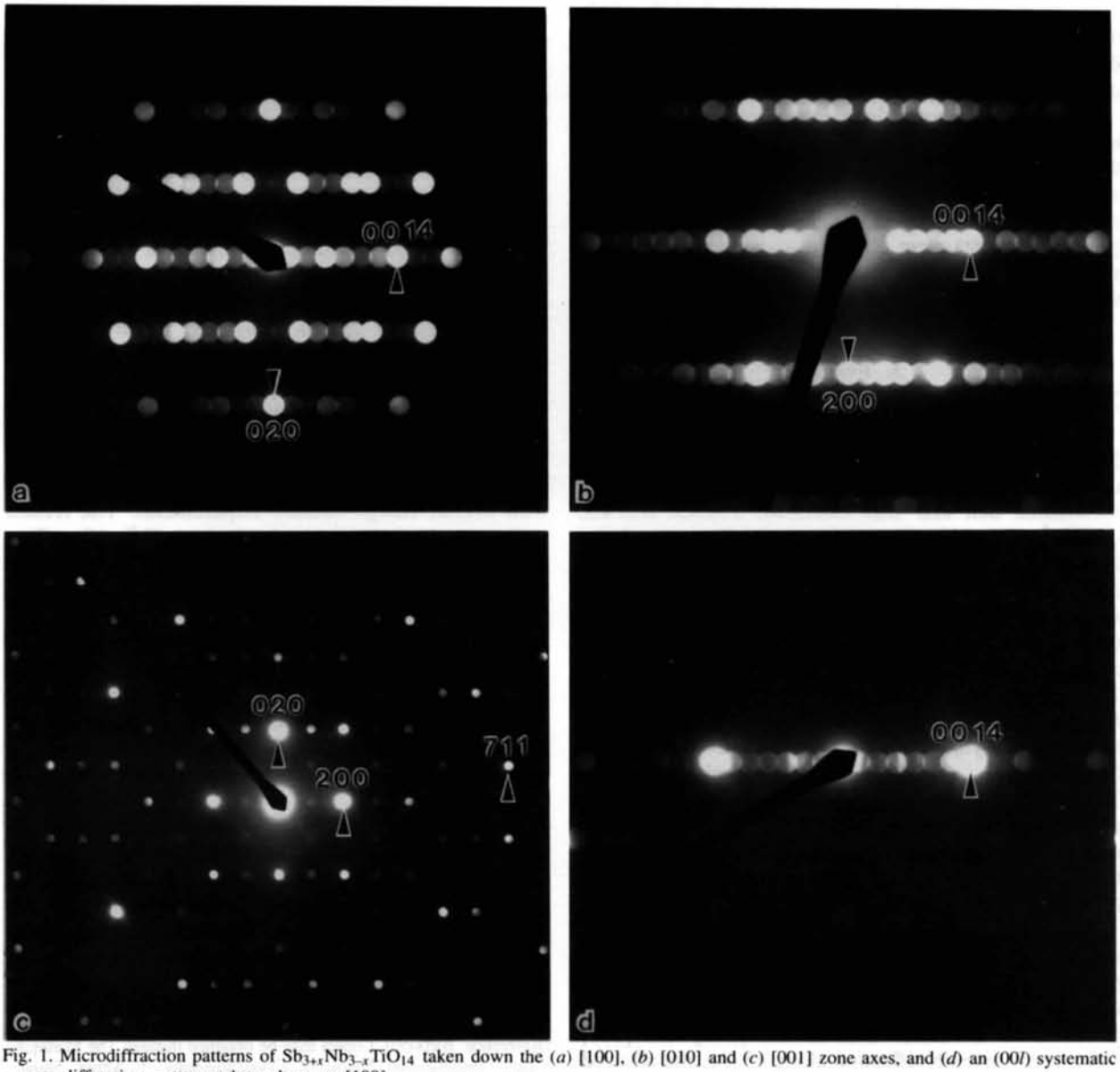

Fig. 1. Microdiffraction patterns of $Sb_{3+x}Nb_{3-x}TiO_{14}$ taken down the (*a*) [100], (*b*) [010] and (*c*) [001] zone axes, and (*d*) an (00*l*) systematic row diffraction pattern taken close to [100].

Table 1. *Experimental details*

	$Sb_{3+x}Nb_{3-x}TiO_{14}$	$Sb_{3+x}Ta_{3-x}TiO_{14}$
Crystal data		
Chemical formula	$Sb_{3.89}Nb_{2.11}TiO_{14}$	$Sb_{4.26}Ta_{1.74}TiO_{14}$
Chemical formula weight	941.5	1105.4
Cell setting	Monoclinic	Monoclinic
Space group	$A2/a$	$A2/a$
a (Å)	5.5190 (6)	5.4920 (5)
b (Å)	4.8650 (5)	4.8370 (5)
c (Å)	40.256 (4)	40.165 (4)
β (°)	91.020 (9)	91.080 (9)
V (Å^3)	1080.7 (2)	1066.8 (2)
Z	4	4
D_x (Mg m^{-3})	5.79	6.88
Radiation type	Mo $K\alpha$	Mo $K\alpha$
Wavelength (Å)	0.7107	0.7107
No. of reflections for cell parameters	25	25
θ range (°)	11.61–26.86	11.60–24.70
μ (mm^{-1})	12.63	30.94
Temperature (K)	293	293
Crystal form	Plate	Plate
Crystal size (mm)	0.2 × 0.2 × 0.018	0.04 × 0.03 × 0.006
Crystal colour	Yellow	Yellow
Data collection		
Diffractometer	Philips PW100	Philips PW100
Data collection method	$\omega/2\theta$ scans	$\omega/2\theta$ scans
Absorption correction	Gaussian	Gaussian
T_{min}	0.1470	0.4168
T_{max}	0.7913	0.7878
No. of measured reflections	5060	4547
No. of independent reflections	2375	2346
No. of observed reflections	2151	1912
Criterion for observed reflections	Reflections observed if $F > 3\sigma(F)$	Reflections observed if $F > 3\sigma(F)$
R_{int}	0.028	0.041
θ_{max} (°)	35	34.97
Range of h, k, l	$-8 \rightarrow h \rightarrow 0$ $-7 \rightarrow k \rightarrow 0$ $-64 \rightarrow l \rightarrow 63$	$-8 \rightarrow h \rightarrow 0$ $-7 \rightarrow k \rightarrow 0$ $-64 \rightarrow l \rightarrow 63$
No. of standard reflections	3	3
Frequency of standard reflections (min)	120	120
Intensity decay (%)	None	0.1
Refinement		
Refinement on	F	F
R	0.047	0.063
wR	0.034	0.08
S	4.238	4.504
No. of reflections used in refinement	2151	1912
No. of parameters used	99	64
Weighting scheme	σ	σ
$(\Delta/\sigma)_{max}$	0.002	0.07
$\Delta\rho_{max}$ (e Å^{-3})	7.00	10.252
$\Delta\rho_{min}$ (e Å^{-3})	−5.22	−6.841
Extinction method	Zachariasen (1968)	Zachariasen (1968)
Extinction coefficient	1421 (116)	13 930 (889)
Source of atomic scattering factors	*International Tables for X-ray Crystallography* (1974, Vol IV, Tables 2.2B and 2.3.1)	*International Tables for X-ray Crystallography* (1974, Vol IV, Tables 2.2B and 2.3.1)
Computer programs		
Data reduction	*Xtal DIFDAT*, *ADDREF*, *ABSORB*, *SORTRF* (Hall, Flack & Stewart, 1992)	*Xtal DIFDAT*, *ADDREF*, *ABSORB*, *SORTRF* (Hall *et al.*, 1992)
Structure solution	*Xtal* (Hall *et al.*, 1992)	*Xtal* (Hall *et al.*, 1992)
Structure refinement	*Xtal CRYLSQ* (Hall *et al.*, 1992)	*Xtal CRYLSQ* (Hall *et al.*, 1992)
Preparation of material for publication	*Xtal BONDLA*, *CIFIO* (Hall *et al.*, 1992)	*Xtal BONDLA*, *CIFIO* (Hall *et al.*, 1992)

about a clearly visible in Fig. 2(*a*). While octahedral rotation modes are common to most Aurivillius phases, the magnitudes of the rotation angles are always much smaller (< 10°; Withers *et al.*, 1991). These rotations generate an approximately h.c.p. oxygen array (a 30° rotation effecting complete transformation from the perovskite structure to an h.c.p. anion array; Hyde & Andersson, 1989*a*). Successive corner-connected octahedral layers of the type shown in Fig. 2(*a*) would in any event leave no room for the perovskite *A* cation of an Aurivillius-type structure, with the possible exception of Li^+ (*cf.* the structure of $LiNbO_3$; Hyde & Andersson,

Table 2. *Fractional atomic coordinates and equivalent isotropic displacement parameters (Å²) for* $Sb_{3+x}Nb_{3-x}TiO_{14}$

$U_{eq} = (1/3)\Sigma_i\Sigma_j U_{ij} a_i^* a_j^* \mathbf{a}_i.\mathbf{a}_j.$

	Occupancy	x	y	z	U_{eq}
Sb1	1.0	0.76043 (6)	0.29419 (7)	0.85409 (1)	0.0137 (2)
Sb2	1.0	3/4	0.7052 (1)	0.50000	0.0138 (2)
Nb5	0.92	0.63252 (7)	0.75283 (9)	0.92697 (1)	0.0089 (2)
Sb5	0.08	0.63252 (7)	0.75283 (9)	0.92697 (1)	0.0089 (2)
Nb4	0.14	0.82774 (8)	0.7554 (1)	0.78216 (2)	0.0091 (3)
Ti4	0.50	0.82774 (8)	0.7554 (1)	0.78216 (2)	0.0091 (3)
Sb4	0.36	0.82774 (8)	0.7554 (1)	0.78216 (2)	0.0091 (3)
O1	1.0	0.5792 (6)	0.4207 (8)	0.4719 (1)	0.011 (2)
O2	1.0	0.9087 (6)	0.0844 (8)	0.3247 (1)	0.010 (2)
O3	1.0	0.5872 (6)	0.0801 (8)	0.3808 (1)	0.012 (2)
O4	1.0	0.8514 (5)	0.4354 (8)	0.2370 (1)	0.009 (2)
O5	1.0	0.8765 (6)	0.0183 (9)	0.4420 (1)	0.012 (2)
O6	1.0	0.8339 (6)	0.5315 (8)	0.4108 (1)	0.014 (2)
O7	1.0	0.5663 (6)	0.4521 (8)	0.2959 (1)	0.010 (2)

1989*b*). Other differences between these and Aurivillius phases include the simultaneous existence of single and double octahedral layer slabs and the quite different nature of the discrete Sb^{3+} and $Bi_2O_2^{2+}$ layers.

The structure may be most succinctly described as an ordered intergrowth of slabs of the (monoclinic) β-Sb_2O_4 structure [the region $Sb^{III}1$, O3, O6, $Sb^{V}Nb$,

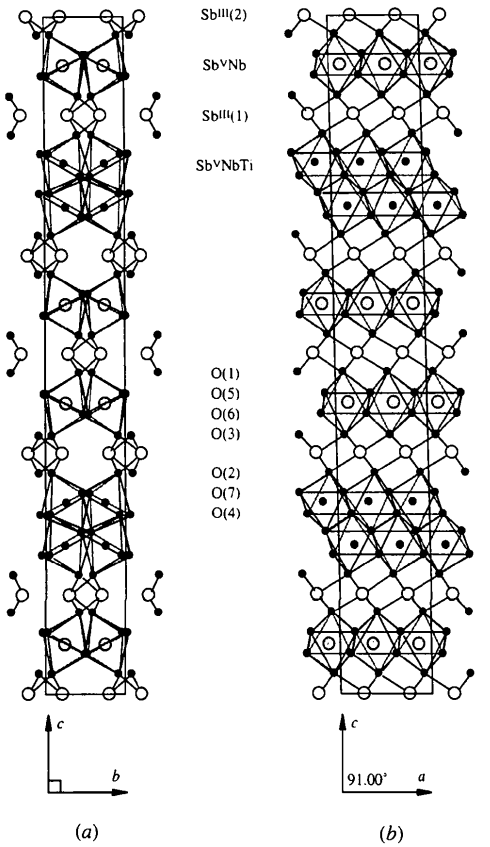

(*a*) (*b*)

Fig. 2. (*a*) [100] and (*b*) [010] zone-axis projections of $Sb_{3+x}Nb_{3-x}TiO_{14}$, $x = 0.89$.

Table 3. *Bond lengths (Å) for* $Sb_{3+x}Nb_{3-x}TiO_{14}$

Sb1^{i}—O2	2.024 (4)	Sb5^{i}—O6^{vii}	2.050 (4)
Sb1^{i} O3	2.010 (4)	Nb4^{i}— O2	1.948 (4)
Sb1^{i}—O2^{ii}	2.331 (3)	Nb4^{i}—O4	2.024 (4)
Sb1^{i}—O3^{iii}	2.171 (4)	Nb4^{i}—O7	1.825 (4)
Sb2—O1	2.011 (4)	Nb4^{i}—O7^{iv}	2.010 (4)
Sb2—O1^{iv}	2.242 (4)	Nb4^{i}—O4^{viii}	2.155 (3)
Sb2—O1^{v}	2.242 (4)	Nb4^{i}—O4^{ix}	1.992 (4)
Sb2—O1^{vi}	2.011 (4)	Ti4^{i}—O2	1.948 (4)
Nb5^{i}—O1	2.011 (4)	Ti4^{i}—O4	2.024 (4)
Nb5^{i}—O3	2.051 (4)	Ti4^{i}—O7	1.825 (4)
Nb5^{i}—O5	1.858 (4)	Ti4^{i}—O7^{iv}	2.010 (4)
Nb5^{i}—O6	1.876 (4)	Ti4^{i}—O4^{viii}	2.155 (3)
Nb5^{i}—O5^{ii}	2.034 (4)	Ti4^{i}—O4^{ix}	1.992 (4)
Nb5^{i}—O6^{vii}	2.050 (4)	Sb4^{i}—O2	1.948 (4)
Sb5^{i}—O1	2.011 (4)	Sb4^{i}—O4	2.024 (4)
Sb5^{i}—O3	2.051 (4)	Sb4^{i}—O7	1.825 (4)
Sb5^{i}—O5	1.858 (4)	Sb4^{i}—O7^{iv}	2.010 (4)
Sb5^{i}—O6	1.876 (4)	Sb4^{i}—O4^{viii}	2.155 (3)
Sb5^{i}—O5^{ii}	2.034 (4)	Sb4^{i}—O4^{ix}	1.992 (4)

Symmetry codes: (i) $x, y - \frac{1}{2}, z - \frac{1}{2}$; (ii) $x - \frac{1}{2}, -y, z$; (iii) $\frac{1}{2} + x, -y, z$; (iv) $\frac{1}{2} + x, 1 - y, z$; (v) $1 - x, 1 - y, 1 - z$; (vi) $\frac{3}{2} - x, y, 1 - z$; (vii) $x - \frac{1}{2}, 1 - y, z$; (viii) $2 - x, \frac{1}{2} - y, \frac{1}{2} - z$; (ix) $\frac{3}{2} - x, y - \frac{1}{2}, \frac{1}{2} - z$.

Table 4. *Fractional atomic coordinates and equivalent isotropic displacement parameters (Å²) for* $Sb_{3+x}Ta_{3-x}TiO_{14}$

$U_{eq} = (1/3)\Sigma_i\Sigma_j U_{ij} a_i^* a_j^* \mathbf{a}_i.\mathbf{a}_j.$

	Occupancy	x	y	z	U_{eq}
Sb1	1.0	0.7568 (3)	0.2919 (2)	0.85362 (3)	0.0098 (5)
Sb2	1.0	3/4	0.7086 (3)	1/2	0.0093 (8)
Ta5	0.41	0.6233 (2)	0.7507 (2)	0.92696 (2)	0.0037 (4)
Sb5	0.59	0.6233 (2)	0.7507 (2)	0.92696 (2)	0.0037 (4)
Ta4	0.46	0.8333 (2)	0.7582 (2)	0.78210 (3)	0.0052 (5)
Ti4	0.50	0.8333 (2)	0.7582 (2)	0.78210 (3)	0.0052 (5)
Sb4	0.04	0.8333 (2)	0.7582 (2)	0.78210 (3)	0.0052 (5)
O1	1.0	0.573 (2)	0.418 (2)	0.4723 (3)	0.005 (2)
O2	1.0	0.907 (3)	0.084 (3)	0.3254 (4)	0.009 (2)
O3	1.0	0.596 (2)	0.080 (2)	0.3807 (3)	0.006 (2)
O4	1.0	0.858 (2)	0.436 (2)	0.2364 (3)	0.005 (2)
O5	1.0	0.880 (3)	0.020 (2)	0.4432 (4)	0.008 (2)
O6	1.0	0.836 (2)	0.532 (3)	0.4107 (3)	0.008 (2)
O7	1.0	0.573 (2)	0.448 (2)	0.2962 (3)	0.005 (2)

Table 5. *Bond lengths (Å) for* $Sb_{3+x}Ta_{3-x}TiO_{14}$

Sb1^{i}—O2	2.00 (1)	Sb5^{i}—O6^{vii}	2.00 (1)
Sb1^{i}—O3	1.99 (1)	Ta4^{i}—O2	1.97 (1)
Sb1^{i}—O2^{ii}	2.29 (1)	Ta4^{i}—O4	2.03 (1)
Sb1^{i} O3^{iii}	2.23 (1)	Ta4^{i} O7	1.80 (1)
Sb2—O1	2.03 (1)	Ta4^{i}—O7^{iv}	2.01 (1)
Sb2—O1^{iv}	2.20 (1)	Ta4^{i}—O4^{viii}	2.09 (1)
Sb2—O1^{v}	2.20 (1)	Ta4^{i}—O4^{ix}	2.01 (1)
Sb2—O1^{vi}	2.03 (1)	Ti4^{i}—O2	1.97 (1)
Ta5^{i}—O1	2.01 (1)	Ti4^{i}—O4	2.03 (1)
Ta5^{i}—O3	2.04 (1)	Ti4^{i}—O7	1.80 (1)
Ta5^{i}—O5	1.90 (1)	Ti4^{i}—O7^{iv}	2.01 (1)
Ta5^{i}—O6	1.92 (1)	Ti4^{i}—O4^{viii}	2.09 (1)
Ta5^{i}—O5^{ii}	1.99 (1)	Ti4^{i}—O4^{ix}	2.01 (1)
Ta5^{i}—O6^{vii}	2.00 (1)	Sb4^{i}—O2	1.97 (1)
Sb5^{i}—O1	2.01 (1)	Sb4^{i}—O4	2.03 (1)
Sb5^{i}—O3	2.04 (1)	Sb4^{i}—O7	1.80 (1)
Sb5^{i}—O5	1.90 (1)	Sb4^{i}—O7^{iv}	2.01 (1)
Sb5^{i}—O6	1.92 (1)	Sb4^{i}—O4^{viii}	2.09 (1)
Sb5^{i}—O5^{ii}	1.99 (1)	Sb4^{i}—O4^{ix}	2.01 (1)

Symmetry codes: (i) $x, y - \frac{1}{2}, z - \frac{1}{2}$; (ii) $x - \frac{1}{2}, -y, z$; (iii) $\frac{1}{2} + x, -y, z$; (iv) $\frac{1}{2} + x, 1 - y, z$; (v) $1 - x, 1 - y, 1 - z$; (vi) $\frac{3}{2} - x, y, 1 - z$; (vii) $x - \frac{1}{2}, 1 - y, z$; (viii) $2 - x, \frac{1}{2} - y, \frac{1}{2} - z$; (ix) $\frac{3}{2} - x, y - \frac{1}{2}, \frac{1}{2} - z$.

Table 6. *Bond valence sums (Brese & O'Keeffe, 1991) for possible metal atoms on the four refined metal sites in the refined structure of* $Sb_{3+x}Nb_{3-x}TiO_{14}$

	Sb^{III}	Sb^{V}	Nb^{V}	Ti^{IV}
$Sb^{III}1$	2.99	2.66	2.45	1.89
$Sb^{III}2$	2.95	2.71	2.50	1.92
$Sb^{V}_{0.08}Nb_{0.92}$	6.03	5.54	5.09	3.93
$Sb^{V}_{0.36}Nb_{0.14}Ti_{0.5}$	5.90	5.43	4.99	3.85

Table 7. *Bond valence sums (Brese & O'Keeffe, 1991) for possible metal atoms on the four refined metal sites in the refined structure of* $Sb_{3+x}Ta_{3-x}TiO_{14}$

	Sb^{III}	Sb^{V}	Ta^{V}	Ti^{IV}
$Sb^{III}1$	3.00	2.76	2.60	1.96
$Sb^{III}2$	2.99	2.75	2.54	1.95
$Sb^{V}_{0.59}Ta_{0.41}$	6.03	5.54	5.22	3.93
$Sb^{V}_{0.04}Ta_{0.46}Ti_{0.5}$	6.00	5.51	5.20	3.91

Table 8. U_{ij} *displacement parameters* (10^{-3} Å^2) *for* $Sb_{3+x}Nb_{3-x}TiO_{14}$, $x = 0.89$

	U_{11}	U_{22}	U_{33}	U_{12}	U_{13}	U_{23}
$Sb^{III}1$	12.3 (1)	6.3 (1)	22.7 (3)	−1.3 (1)	5.7 (1)	−3.6 (2)
$Sb^{III}2$	15.1 (2)	5.9 (2)	20.0 (3)	0	−6.5 (2)	0
$Sb^{V}_{0.08}Nb_{0.92}$	7.4 (2)	5.7 (2)	13.7 (3)	0.1 (1)	0.4 (1)	0.2 (2)
$Sb^{V}_{0.36}Nb_{0.14}Ti_{0.5}$	7.4 (2)	6.1 (2)	13.8 (3)	0.9 (2)	−0.6 (2)	−0.4 (2)
O1	9 (1)	11 (2)	14 (2)	−1 (1)	1 (1)	−3 (2)
O2	8 (1)	7 (1)	17 (2)	−2 (1)	4 (1)	4 (2)
O3	5 (1)	7 (1)	23 (2)	3 (1)	−4 (1)	−6 (2)
O4	5 (1)	5 (1)	18 (2)	1 (1)	−1 (1)	0 (2)
O5	11 (1)	11 (2)	14 (2)	6 (1)	−2 (1)	−1 (2)
O6	8 (1)	11 (2)	24 (3)	−6 (1)	−3 (1)	−1 (2)
O7	7 (1)	6 (1)	17 (2)	2 (1)	0 (1)	0 (2)

Table 9. U_{ij} *and* U_{iso} *displacement parameters* (10^{-3} Å^2) *for* $Sb_{3+x}Nb_{3-x}TiO_{14}$, $x = 1.26$

	$U_{11/iso}$	U_{22}	U_{33}	U_{12}	U_{13}	U_{23}
$Sb^{III}1$	14.1 (6)	2.3 (4)	13.1 (6)	−0.9 (4)	4.3 (4)	−2.1 (4)
$Sb^{III}2$	14 (1)	2.7 (6)	11.2 (8)	0 (-)	−5.7 (6)	0 (-)
$Sb^{V}_{0.41}Ta_{0.92}$	5.9 (4)	0.5 (3)	4.8 (4)	0.0 (3)	−0.2 (3)	−0.1 (3)
$Sb^{V}_{0.04}Ta_{0.46}Ti_{0.5}$	7.0 (6)	2.2 (5)	6.5 (6)	0.1 (4)	−1.4 (4)	0.1 (4)

O5, O1, $Sb^{III}2$, O1, O5, Sb^{V}Nb, O6, O3, $Sb^{III}1$ (Rogers & Skapski, 1964)] and the Sb_2O_5 structure [the region O2, O7, Sb^{V}(Nb,Ta)Ti, O4, O4, Sb^{V}(Nb,Ta)Ti, O7, O2 (Andersson & Åström, 1972)]. From the [010] zone-axis projection (Fig. 2*b*) a more subtle feature of the structure may be seen; all $Sb^{III}1$ slabs function as boundary planes between β-Sb_2O_4 and Sb_2O_5 units, on which the angle between the normal to the pseudo-h.c.p. oxygen array and the *c*-axis changes sign. These boundary planes are analogous to the ordered twin planes found in (orthorhombic) α-Sb_2O_4 (Skapski & Rogers, 1965), where they occur on all $Sb^{III}2$-type slabs.

Systematically high values of U_{33} compared with U_{11} and U_{22} for metal atoms in both structures (see Tables 8 and 9) indicate concerted layer–layer motion. This is explainable in terms of occasional stacking faults between the component structure types. Also noticeable in Tables 8 and 9 are systematically large U_{11}, U_{33} and U_{13} values for the Sb^{III} sites, indicating preferential motion along the Sb^{III}—O bonds. This suggests that metals in the Sb^{III} slabs (pseudo-tetragonal coordination) are less rigidly bound than those in the octahedral sites. The only departure from these trends is shown by the very low U_{22} value for the Sb^{V}/Ta mixed-metal site, which can only be explained as an artifact in the refinement of the lesser quality data obtained from this crystal.

The mixed-atom sites involve elements found in phases isostructural with the primary oxides of antimony discussed above, *e.g.* $SbNbO_4$ is isostructural with α-Sb_2O_4 (Hyde & Andersson, 1989*b*) and β-Nb_2O_5 is isostructural with Sb_2O_5 (Andersson & Åström, 1972). Titanium, required for charge balance in this arrangement of slabs, is present in the Sb_2O_5 unit, which is analogous to two layers of the rutile (TiO_2) structure. The solid solution ranges are necessarily limited by complete occupancy of these sites by either Sb^{V} or Nb/Ta, *i.e.* $0 \le x \le 3$. Further work is needed, however, to determine the explicitly accessible range of x.

It is, therefore, possible to describe the structure of $Sb_{3+x}Nb_{3-x}TiO_{14}$ and $Sb_{3+x}Ta_{3-x}TiO_{14}$ in terms of ordered intergrowths of slabs of the primary oxides of antimony, with the other metal atoms mixed onto sites analogous to those found in their own primary oxides or binary oxides with Sb^{V}. Nb^{V}/Ta^{V} substitutes for Sb^{V} in β-Sb_2O_4-type slabs and Nb^{V}/Ta^{V}/Ti^{IV} substitutes for Sb^{V} in Sb_2O_5-type slabs. This constitutes a new type of layered intergrowth structure, based almost exclusively on simple antimony oxide structures, but combined in a surprisingly complex manner.

References

Andersson, S. & Åström, A. (1972). *Natl. Bur. Standards, 5th Mat. Symp.* pp. 3–14.

Aurivillius, B. (1949). *Arkiv. Kemi*, **1**, 463–480.

Brese, N. E. & O'Keefe, M. (1991). *Acta Cryst.* B**47**, 192–197.

Castro, A., Millán, P., Enjalbert, R., Snoeck, E. & Galy, J. (1994). *Mat. Res. Bull.* **29**, 871–879.

Castro, A., Millán, P. & Martinez-Lope, M. J. (1993*a*). *Solid State Ion.* pp. 63–65.

Castro, A., Millán, P. & Martinez-Lope, M. J. (1993*b*). *Solid State Ion.* pp. 897–901.

Hall, S. R., Flack, H. D. & Stewart, J. M. (1992). Editors. *Xtal3.2 Reference Manual.* Universities of Western Australia, Australia, Geneva, Switzerland, and Maryland, USA.

Hyde, B. G. & Andersson, S. (1989*a*). *Inorganic Crystal Structures*, pp. 299–300. New York: Wiley.

Hyde, B. G. & Andersson, S. (1989*b*). *Inorganic Crystal Structures*, pp. 260–265. New York: Wiley.

Lee, K. L., Lim, G. S. & West, A. R. (1994). *J. Mater. Chem.* **4**, 1441–1444.
Ling, C. D., Withers, R. L., Rae, A. D., Schmid, S. & Thompson, J. G. (1996). *Acta Cryst.* B**52**, 610–615.
Palmer, D. C. (1994). *CrystalMaker*. Lynxvale Ltd, Cambridge.
Rae, A. D., Thompson, J. G. & Withers, R. L. (1991). *Acta Cryst.* B**47**, 870–881.
Rae, A. D., Thompson, J. G. & Withers, R. L. (1992). *Acta Cryst.* B**48**, 418–428.
Rogers, D. & Skapski, A. C. (1964). *Proc. Chem. Soc.* pp. 400–401.
Singh, K., Bopardikare, D. K. & Atkare, D. V. (1988). *Ferroelectrics*, **82**, 55–67.
Skapski, A. C. & Rogers, D. (1965). *Chem. Commun.* pp. 611–613.
Subbanna, G. N., Ganapathi, L., Rao, C. N. R. & Jefferson, D. A. (1986). *Mat. Res. Bull.* **22**, 205–209.
Subbarao, E. C. (1973). *Ferroelectrics*, **5**, 267–280.
Thompson, J. G., Rae, A. D., Withers, R. L. & Craig, D. C. (1991). *Acta Cryst.* B**47**, 174–180.
Withers, R. L., Thompson, J. G. & Rae, A. D. (1991). *J. Solid State Chem.* **94**, 404–417.
Zachariasen, W. H. (1968). *Acta Cryst.* A**24**, 212–216.